

Equation of state constraints from the threshold binary mass for prompt collapse of neutron star mergers

Andreas Bauswein,¹ Sebastian Blacker,^{1,2} Vimal Vijayan,¹ Nikolaos Stergioulas,³ Katerina Chatziioannou,⁴ James A. Clark,⁵ Niels-Uwe F. Bastian,⁶ David B. Blaschke,^{6,7,8} Mateusz Cieniak,⁶ and Tobias Fischer⁶

¹*GSI Helmholtzzentrum für Schwerionenforschung, Planckstraße 1, 64291 Darmstadt, Germany*

²*Institut für Kernphysik, Technische Universität Darmstadt, 64289 Darmstadt, Germany*

³*Department of Physics, Aristotle University of Thessaloniki, 54124 Thessaloniki, Greece*

⁴*Center for Computational Astrophysics, Flatiron Institute, 162 5th Ave, New York, NY 10010, USA*

⁵*Center for Relativistic Astrophysics, School of Physics,*

Georgia Institute of Technology, Atlanta, Georgia 30332, USA

⁶*Institute of Theoretical Physics, University of Wrocław, 50-205 Wrocław, Poland*

⁷*National Research Nuclear University (MEPhI), 115409 Moscow, Russia*

⁸*Bogoliubov Laboratory for Theoretical Physics, Joint Institute for Nuclear Research, 141980 Dubna, Russia*

(Dated: October 7, 2020)

Using hydrodynamical simulations for a large set of high-density matter equations of state (EoSs) we systematically determine the threshold mass M_{thres} for prompt black-hole formation in equal-mass and asymmetric neutron star (NS) mergers. We devise the so far most direct, general and accurate method to determine the unknown maximum mass of nonrotating NSs from merger observations revealing M_{thres} . Considering hybrid EoSs with hadron-quark phase transition, we identify a new, observable signature of quark matter in NS mergers. Furthermore, our findings have direct applications in gravitational wave searches, kilonova interpretations and multi-messenger constraints on NS properties.

PACS numbers: 04.30.Tv, 26.60.Kp, 26.60Dd, 97.60.Jd

Motivation and context: With the sensitivity increase of current gravitational-wave (GW) detectors, observations of neutron star (NS) mergers will become routine in the very near future [1, 2]. Also, the identification of electromagnetic counterparts will succeed frequently as sky localizations from the GW signal improve, more dedicated instruments become operational and observing strategies advance. This includes the radiation from ejecta in the ultraviolet, optical and infrared wavebands, so-called kilonovae [3], but also gamma ray, X-ray and radio emission from relativistic outflows [4].

One of the most basic features of a NS coalescence is the immediate merger product, which can either be a black hole (BH) for high total binary masses or a NS remnant for lower total masses [5–8]. The latter may undergo a delayed collapse to a BH. Generally, the NS remnant’s lifetime increases with decreasing total binary mass [9–17].

Based on the distinction between prompt and delayed BH formation for systems with different total binary mass, one can introduce a threshold binary mass M_{thres} for direct collapse, which is measurable. The total binary mass M_{tot} can be inferred with good precision from the inspiral GW signal, i.e. the premerger phase¹. The merger outcome can be observationally discerned either

by the presence of strong postmerger GW emission from a NS remnant [19, 20] (absent for direct BH formation) or from the properties of the electromagnetic counterpart, which is expected to be relatively dim for prompt-collapse events because of reduced mass ejection [21–23]. Thus, a number of measurements with different M_{tot} and information on the merger product yields M_{thres} . The measurement uncertainty essentially depends on how the detections sample the M_{tot} range. It should thus continuously decrease with the number of events which allow a distinction between the possible outcomes.

The threshold binary mass is highly important for the interpretation of NS merger observations [2, 3, 18, 23–36]. Moreover, M_{thres} depends in a specific way on the incompletely known equation of state (EoS) of NS matter [8]. Therefore, understanding the EoS dependence of the collapse behavior is crucial for current and future constraints on unknown properties of high-density matter and of NSs, such as their maximum mass [8], radii [37–39] and tidal deformabilities [13, 40–42]. The prospect to determine M_{max} is very notable, where solid lower limits are currently provided by pulsar measurements [43–45]. Upper limits are inferred through more elaborated interpretations of observational data indicating a finite remnant lifetime, e.g. [23, 46–55]. Estimates of the remnant’s late-time behavior may be subject to considerable model dependencies. The present paper instead deals with the threshold for direct BH formation, which leads to different, relatively strong and clear observational features. Apart from implications for high-density matter physics [56–58], M_{max} is also crucial for BH formation in

¹ In practice, the chirp mass is measured with very high precision and constraints on the binary mass ratio are required to obtain M_{tot} [1, 18].

core-collapse supernovae and BH physics [59–64].

In this Letter we determine the impact of the properties of high-density matter on the threshold binary mass for prompt BH collapse. We go beyond current knowledge in several respects. We consider the so far largest sample of EoSs to determine M_{thres} and find new, tight relations describing its EoS dependence. For the first time, we systematically determine binary mass ratio effects on M_{thres} . Furthermore, we investigate the impact of phase transitions on the collapse behavior.

We put forward four main applications of our new findings:

1) Along the lines of [8] we devise a more direct, more general and more accurate method to determine M_{max} from NS merger observations providing information about the immediate merger outcome and about the total binary mass and combined tidal deformability from the inspiral GW signal.

2) We identify a new signature of a phase transition to deconfined quark matter in NS mergers. This stresses the enormous potential of future merger observations [65–86] to understand the phase diagram of matter in the non-perturbative regime of finite chemical potentials, which is not accessible by ab-initio QCD calculations [87, 88]. Currently, it is not known whether the hadron-quark phase transition takes place at typical NS densities. Identifying an imprint of the phase transition in merger observables will thus also provide invaluable insights for heavy-ion experiments, which will explore the phase diagram at such densities and finite temperature (but different isospin) [89–91].

3) Beyond these future prospects, our novel, more general relations are directly applicable in detection and analysis pipelines to quantify the likelihood of a specific merger outcome and thus for instance GW and kilonova characteristics [2, 3, 23, 26, 30–34, 92–96].

4) Furthermore, they are key input for current multimessenger constraints on NS properties as in [37–42].

See e.g. [23, 26, 27, 30–33, 37–39, 94–96] for concrete implementations of M_{thres} dependencies. These applications can be significantly improved by the findings in this study. Below we describe our results mostly in the context of the first two applications.

Simulations and setup: We perform three-dimensional relativistic hydrodynamical simulations of NS mergers for a large set of different EoSs of NS matter. For every EoS, we compute $M_{\text{thres}}(\text{EoS}; q)$ for fixed binary mass ratios $q = M_1/M_2 = 1$ and $q = 0.7$. Masses M_1 and M_2 of the individual binary components, M_{tot} and M_{thres} refer to the gravitational mass (for binaries at infinite orbital separation). Simulations start from quasi-equilibrium circular orbits a few revolutions before merger, with stars initially at zero temperature and in neutrino-less beta-equilibrium. The merger calculations are conducted with a relativistic smooth particle hydrodynamics code, which adopts the spatial conformal flatness condition to solve

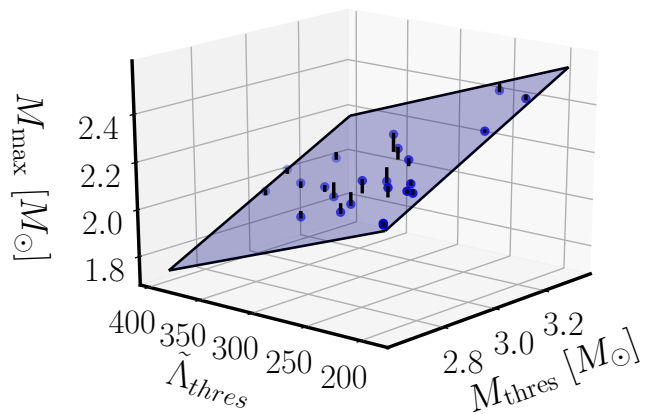


FIG. 1: Maximum mass M_{max} of nonrotating NSs as function of the threshold binary mass M_{thres} for prompt BH formation and combined tidal deformability $\Lambda_{\text{thres}} = \hat{\Lambda}(M_{\text{thres}}/2)$ of the binary at the threshold for direct collapse. Blue plane shows a bilinear fit to the data for $q = 1$. Short black lines visualize the deviation between fit (blue plane) and data points.

the Einstein field equations [97, 98]. More details on the simulation tool, comparisons to other codes (showing generally a very good agreement) and resolution studies can be found in [8, 32, 37, 38, 99–104].

In this study we consider 23 different hadronic EoSs [62, 105–124], which constitute our “base sample” and are consistent with astrophysical constraints from [1, 43, 44]. To enlarge the parameter space, we optionally supplement those with 8 additional hadronic EoSs [115–118, 125–128] which are incompatible with the tidal deformability constraints from GW170817 [1]. Among all these EoSs five models include hyperons. Additionally, we consider 9 hybrid models with a first-order phase transition to deconfined quark matter leading to a strong softening of the EoS [68, 111, 129–132]. These models vary in the onset density, the latent heat and the stiffness of quark matter [68, 86]. Among all 40 EoSs, 26 are fully temperature dependent. The remaining models are supplemented with an approximate treatment of thermal effects [101]. We refer to the Supplemental Material, which provides more details on the simulations and the different sets of EoS models and includes Refs. [133–137]. We emphasize that our base sample covers well the full range of viable hadronic models.

M_{max} determination: We first consider results for the base sample of purely hadronic EoSs assuming that indications of a strong phase transition to quark matter may be independently provided by other observations or experiments [68, 75, 76, 89, 132]. We further justify this assumption below by describing a new detectable signature of a phase transition.

Compiling the data for equal-mass mergers, Fig. 1 reveals a tight relation between the maximum mass M_{max} of nonrotating NSs, the threshold binary mass M_{thres}

and $\tilde{\Lambda}_{\text{thres}}$. The latter is the combined tidal deformability of the binary system at the threshold mass, i.e. $\tilde{\Lambda}_{\text{thres}} \equiv \Lambda(M_{\text{thres}}/2)$ for $q = 1$. $\tilde{\Lambda}$ describes the dominant EoS effects during the GW inspiral and is thus measurable [1, 18, 138–146]. It is defined by $\tilde{\Lambda} = \frac{16}{13(M_1+M_2)^5}((M_1+12M_2)M_1^4\Lambda_1 + (M_2+12M_1)M_2^4\Lambda_2)$ with tidal deformabilities $\Lambda_{1(2)}$ of the individual binary components [147–149]. $\Lambda(M)$ is a stellar structure parameter and fully determined by the EoS through $\Lambda_{1(2)} = \frac{2}{3}k_2(R_{1(2)}/M_{1(2)})^5$ with the tidal Love number $k_2(M)$ and stellar radius $R(M)$ (factors of G and c suppressed).

The tidal deformability monotonically decreases with mass. Therefore, $\tilde{\Lambda}_{\text{thres}}$ can be obtained from measurements of systems with different M_{tot} around M_{thres} through a simple interpolation. The tight relation in Fig. 1 implies that a sufficiently accurate measurement of M_{thres} and $\tilde{\Lambda}_{\text{thres}}$ determines the currently unknown maximum mass of nonrotating NSs. The data in Fig. 1 is well described by a bilinear fit

$$M_{\text{max}}(M_{\text{thres}}, \tilde{\Lambda}_{\text{thres}}) = aM_{\text{thres}} + b\tilde{\Lambda}_{\text{thres}} + c, \quad (1)$$

with $a = 0.632$, $b = -0.002 M_{\odot}$ and $c = 0.802 M_{\odot}$. The maximum residual of this fit is only $0.067 M_{\odot}$, implying a potentially very accurate measurement of M_{max} (see Supplemental Material for fits with an enlarged set of EoSs). The average deviation between Eq. (1) and the underlying data is only $0.02 M_{\odot}$. As an example, assuming M_{thres} to be measured within $0.05 M_{\odot}$ and $\tilde{\Lambda}_{\text{thres}}$ within 5%, an error propagation through Eq. (1) yields $\Delta M_{\text{max}} = 0.06 M_{\odot}$.

For $q = 0.7$ we obtain a similarly tight relation for hadronic EoSs with a maximum residual of $0.078 M_{\odot}$ (with fit parameters $a = 0.621$, $b = -0.001 M_{\odot}$, $c = 0.582 M_{\odot}$; Tab. II in Supplemental Material). For the same EoS M_{thres} of asymmetric systems is comparable to the one of equal-mass mergers (either equal or at most $0.2 M_{\odot}$ smaller). Moreover, we find the difference in M_{thres} , i.e. $M_{\text{thres}}(q = 1) - M_{\text{thres}}(q = 0.7)$, to depend systematically on the EoS. See Supplemental Material for more details, a discussion of the systematic impact of the mass ratio and an intuitive explanation.

Based on our models we construct additional bilinear fits (Tab. II in Supplemental Material) quantifying their quality by the maximum residual and the average deviation between fit and data. For these relations we select different subsets of our data motivated by different assumptions on which additional information may be available (e.g. about q or the presence of a phase transition). For instance, we consider only purely hadronic EoS models or a full set of EoSs including hybrid models with phase transitions, or we include binaries with a fixed mass ratio or a range in q . We also employ different independent variables, which may be measured more precisely in comparison to the quantities in Eq. (1). This includes (i) the chirp mass $\mathcal{M}_c = (M_1M_2)^{3/5}/(M_1+M_2)^{1/5}$ if

the mass ratio is not well constrained or strongly differs among the different events which are combined to determine M_{thres} , (ii) the tidal deformability $\Lambda_{1.4}$ of a $1.4 M_{\odot}$ NS, which may be more accurately and independently measured than $\tilde{\Lambda}_{\text{thres}}$, or (iii) the radius $R_{1.6}$ of a $1.6 M_{\odot}$ NS. We stress that cases (ii) and (iii), i.e. fits 8 to 11, are very promising when $\Lambda_{1.4}$ or $R_{1.6}$ are measured in a high SNR GW detection or by another astronomical observation, e.g. by NICER [150–152].

Generally, all these choices lead to tight relations describing the collapse behavior. This is not unexpected considering the previously found relation $M_{\text{thres}} = (-3.606 \frac{GM_{\text{max}}}{c^2 R_{1.6}} + 2.38)M_{\text{max}}$ for a smaller set of EoS models and only equal-mass mergers [8, 153]. NS radii are roughly constant in a considerable mass range around $M_{\text{thres}}/2$ and the tidal deformability is known to scale approximately with NS radii (see also [153] for a semi-analytic model of the collapse behavior). In comparison to previous results, the new relations presented here allow a more direct and more general implementation in analysis pipelines or waveform models because they involve quantities which are directly measurable from the GW inspiral (of the same event) and do not rely on additional information e.g. about $R_{1.6}$. They also include asymmetric binaries. We remark that the functional form of our new fits like Eq. (1) is more physical compared to relations in [8], which features a unphysical decrease of M_{thres} with M_{max} in a very small range of the parameter space. Finally, we directly compare the relations $M_{\text{max}}(M_{\text{thres}}, \tilde{\Lambda}_{\text{thres}})$ (Eq. (1)) and $M_{\text{max}}(M_{\text{thres}}, R_{1.6})$ (inverted relation from [8]). The maximum residual is $0.067 M_{\odot}$ for the new relation compared to $0.26 M_{\odot}$ for the latter. Hence, the relations describing the collapse behavior in this work are significantly more accurate while they even include more models and consider asymmetric mergers.

Physically, relations as Eq. (1) are understandable. M_{thres} is determined by two roughly independent EoS properties, namely $\tilde{\Lambda}_{\text{thres}}$ characterizing the EoS stiffness at moderate densities and M_{max} at very high densities, both of which increase M_{thres} . For fixed M_{thres} this implies that $\tilde{\Lambda}_{\text{thres}}$ has to decrease with M_{max} .

We emphasize that already a single measurement of M_{tot} and $\tilde{\Lambda}$ can yield a strong constraint on M_{max} . Indications for a prompt collapse in a detection imply $M_{\text{tot}} > M_{\text{thres}}$ and $\tilde{\Lambda} < \tilde{\Lambda}_{\text{thres}}$. From this follows through Eq. (1) that the actual maximum mass of nonrotating NSs is smaller than $M_{\text{max}}(M_{\text{tot}}, \tilde{\Lambda})$ (note the minus sign of the fit parameter b). If a measurement provides evidence for no direct BH formation, the maximum mass of NSs has to be larger than $M_{\text{max}}(M_{\text{tot}}, \tilde{\Lambda})$ because $M_{\text{tot}} < M_{\text{thres}}$ and $\tilde{\Lambda} > \tilde{\Lambda}_{\text{thres}}$ ².

² For instance, a prompt (delayed) collapse event with $M_{\text{tot}} =$

Further applications: All aforementioned relations are bilinear and thus easy to invert for other applications requiring for instance M_{thres} or the tidal deformability to be the dependent quantity (applications 3 and 4). We stress that one can exploit our different relations describing the collapse behavior even if some parameters are poorly constrained as for instance in [37–39] yielding a lower bound on NS radii of about 11 km.

Our models also show that the range of $\tilde{\Lambda}_{\text{thres}}$ is relatively large: for equal-mass mergers $200 \lesssim \tilde{\Lambda}_{\text{thres}} \lesssim 450$, whereas $200 \lesssim \tilde{\Lambda}_{\text{thres}} \lesssim 650$ for $q = 0.7$ [104], which is significantly broader than previously assumed (cf. [32, 154, 155]). Hence, only for $\tilde{\Lambda} < 200$ a prompt collapse can be assumed, while depending on q only events with $\tilde{\Lambda} \gtrsim 650$ may safely be classified as no direct collapse. This is for example relevant for kilonova observations and GW searches to determine whether there may be contributions from strong postmerger GW emission. These ranges imply that independent of M_{max} the tidal deformability of a $1.37 M_{\odot}$ NS has to be larger than about 200 following the arguments in Ref. [37, 40, 42, 49] favoring a delayed collapse in GW170817. This limit is less than the one reported in [40, 41], but our data clearly shows that current observations do not exclude EoSs with $\Lambda_{1.37} > 200$ in line with [37, 42, 156].

New signature of phase transition: By additionally considering the results with hybrid EoSs, we identify a new observable signature of the hadron-quark phase transition, which may occur in NSs. Figure 2 shows $\tilde{\Lambda}_{\text{thres}}$ as function of M_{thres} for all EoSs with $q = 1$. It is striking that all 31 purely hadronic models are located below the dashed line given by

$$\tilde{\Lambda}_{\text{thres}}^{\text{hybrid}} = 488(M_{\text{thres}}/M_{\odot}) - 1050, \quad (2)$$

whereas most hybrid models with a phase transition occur above this curve, i.e. at relatively small M_{thres} but larger $\tilde{\Lambda}_{\text{thres}}$. Hence, a combined measurement of $(M_{\text{thres}}, \tilde{\Lambda}_{\text{thres}})$ with $\tilde{\Lambda}_{\text{thres}} > 488(M_{\text{thres}}/M_{\odot}) - 1050$ provides strong evidence for the presence of a phase transition.

A strong phase transition induces a softening of the EoS at higher densities and thus destabilizes the merger product, i.e. yields a relatively small M_{thres} . For most of these models $M_{\text{thres}}/2$ is smaller than the smallest mass M_{onset} at which quark matter appears in nonrotating NSs. Hence, the inspiralling stars are purely hadronic and the corresponding tidal deformability $\tilde{\Lambda}_{\text{thres}}$ does not carry any information about the phase transition and is thus relatively large. To some extent this effect is comparable to results in [68], where a stronger compactification

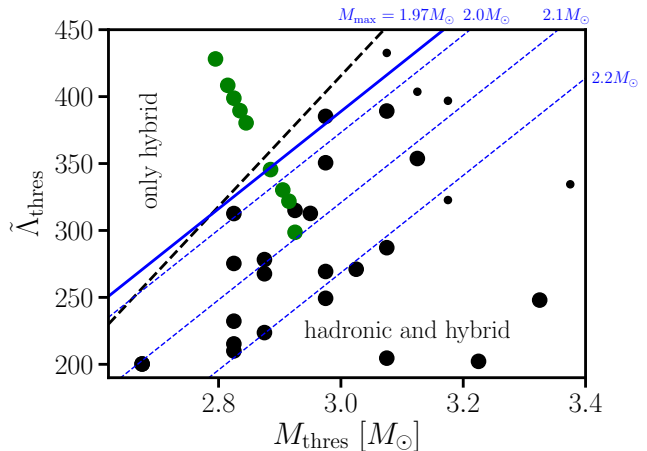


FIG. 2: Combined tidal deformability of binaries at the threshold to prompt BH formation as function of threshold binary mass M_{thres} for direct collapse for different hybrid EoSs (green points) and purely hadronic EoSs (black points; small symbols are models of the “excluded” sample, three outside the plot range). Dashed line indicates boundary beyond which only hybrid models exist (Eq. (2)). In all except for one hybrid model the phase transition occurs after merger. Hence, $\tilde{\Lambda}_{\text{thres}} = \Lambda(M_{\text{thres}}/2)$ is that of purely hadronic stars, which for our models all are described by the same hadronic EoS below the onset density of the phase transition. Therefore, $\tilde{\Lambda}_{\text{thres}}(M_{\text{thres}})$ of these hybrid models appear to line up on a single curve, following $\Lambda(M)$ of the hadronic EoS. The blue lines show curves of constant M_{max} using fit (1) for purely hadronic EoSs explaining the absence of viable hadronic models in the upper left corner.

of the merger remnant by the phase transition leads to a characteristic increase of the postmerger GW frequency.

Figure 2 is a projection of the data point of Fig. 1 onto the $M_{\text{thres}} - \tilde{\Lambda}_{\text{thres}}$ plane. We can thus draw lines of constant M_{max} using fit (1) for purely hadronic EoSs. This explains why no viable purely hadronic EoS models occur above the dash line: Only models with $M_{\text{max}} < 1.97 M_{\odot}$ could yield a $(M_{\text{thres}}, \tilde{\Lambda}_{\text{thres}})$ combination in the upper left corner, which however is excluded by pulsar mass measurements [43, 45]. The situation is different for EoSs with a strong phase transition even if they yield a maximum mass above $2 M_{\odot}$. As explained those models can feature a strong softening at higher densities, which leads to a destabiliation of the merger remnant and a correspondingly low M_{thres} . A low M_{thres} implies that the merging stars of the system with $M_{\text{tot}} = M_{\text{thres}}$ are hadronic and relatively light. This leads to a relatively large $\tilde{\Lambda}_{\text{thres}}$. Thus, hybrid models with this behavior can lead to strong deviations from the $M_{\text{max}}(M_{\text{thres}}, \tilde{\Lambda}_{\text{thres}})$ relation of hadronic EoSs and the data points $(M_{\text{thres}}, \tilde{\Lambda}_{\text{thres}})$ can occur in a regime inaccessible by viable hadronic models.

This explains our finding and solidifies that the de-

3.0 M_{\odot} and $150 < \tilde{\Lambda} < 250$ implies $M_{\text{max}} < 2.40 M_{\odot}$ ($M_{\text{max}} > 2.20$), which may be further tighten by incorporating additional $\tilde{\Lambda}$ data from other events.

scribed signature through the criterion in Eq. (2) is indicative of a phase transition. For $q = 0.7$ we find a qualitatively similar behavior [104].

Following this argumentation we further point out that the limit which indicates a phase transition can be updated when pulsar measurements increase the lower bound on M_{\max} .

We stress several advantages of this new signature to uncover the hadron-quark phase transition in NS mergers. (1) $\tilde{\Lambda}_{\text{thres}}$ does not need to be determined with very high precision in comparison to the accuracy which would be required to detect a relatively weak kink at M_{onset} in $\Lambda(M)$ indicating a phase transition (e.g. Fig. 3 in [42]). A precision of 10% to 30% is sufficient. (2) For most hybrid EoSs studied here $M_{\text{thres}}/2 < M_{\text{onset}}$, which implies that $\tilde{\Lambda}_{\text{thres}}$ is larger than $\Lambda(M_{\text{onset}})$ and thus easier to measure (because of stronger finite-size effects and possibly more frequent systems). Detecting a phase transition with high M_{onset} becomes increasingly challenging for methods employing only the GW inspiral [75, 76], in which case our signature is particularly promising because it is sensitive to the very high-density regime. (3) Already a single measurement with a constraint on $(M_{\text{thres}}, \tilde{\Lambda}_{\text{thres}})$ may reveal indications of a phase transition. (4) M_{tot} can be measured with very good precision and there are a number of different signals potentially revealing the merger product, e.g. postmerger GWs, kilonovae, and possibly gamma-ray bursts, implying that a sufficient M_{thres} determination is conceivable in the near future. In fact, all in principle required observables have already been measured [1, 4].

Notably, not all hybrid EoSs lie in the “hybrid regime” above the dashed line in Fig. 2. These are models with a very strong stiffening of the EoS in the quark phase (with M_{\max} exceeding the one of the purely hadronic reference model; see Supplemental Material). One may refer to this as a coarse variant of the masquerade problem [121], where hybrid models roughly resemble the mass-radius relation of purely hadronic EoSs. The stiffening leads to a stabilization of the merger product and thus to a relatively large M_{thres} and consequently a relatively small $\tilde{\Lambda}_{\text{thres}} \equiv \Lambda(M_{\text{thres}}/2)$. A $(M_{\text{thres}}, \tilde{\Lambda}_{\text{thres}})$ below the dashed curve does thus generally not allow to infer the nature of high-density NS matter. However, the proximity to the dash curve indicates a softening of the EoS at higher densities and possibly the occurrence of a weak phase transition.

Conclusions: Future work should investigate potential systematic uncertainties which might exist on a very low level, overcome those by improved numerical and physical modeling, and explore in more detail the observational features resulting from the collapse behavior. Also, an even larger set of hybrid EoSs should be considered because our current models vary the properties of the quark phase but employ the same hadronic EoS at densities below the phase transition.

This hadronic reference model lies in the middle of the range given by current astrophysical and experimental constraints [1, 37, 43, 44, 58, 146, 157–161]. We thus expect that other hybrid models show the same behavior; such models should essentially be shifted parallel to the dashed line.

Acknowledgements: We thank G. Martinez-Pinedo and H.-T. Janka for helpful discussions. We thank C. Constantinou, M. Prakash, A. Schneider and J. Smith for help with their EoS tables. AB acknowledges support by the European Research Council (ERC) under the European Union’s Horizon 2020 research and innovation programme under grant agreement No. 759253. A.B. and S.B. acknowledge support by Deutsche Forschungsgemeinschaft (DFG, German Research Foundation) - Project-ID 279384907 - SFB 1245. A.B. and V.V. acknowledge support by DFG - Project-ID 138713538 - SFB 881 (“The Milky Way System”, subproject A10). D.B. and T.F. acknowledge support from the Polish National Science Center (NCN) under grant no. 2019/33/B/ST9/03059. T.F. acknowledges support from NCN under Grant No. UMO-2016/23/B/ST2/00720. NUFB acknowledges support from NCN under grant number 2019/32/C/ST2/00556. N.S. is supported by the ARIS facility of GRNET in Athens (SIMGRAV, SIMDIFF and BNSMERGE allocations) and the “Aristoteles Cluster” at AUTH, as well as by the COST actions CA16214 “PHAROS”, CA16104 “GWVerse”, CA17137 “G2Net” and CA18108 “QG-MM”.

-
- [1] B. P. Abbott, R. Abbott, T. D. Abbott, F. Acernese, K. Ackley, C. Adams, T. Adams, P. Addesso, R. X. Adhikari, V. B. Adya, et al. (LIGO Scientific Collaboration and Virgo Collaboration), *Phys. Rev. Lett.* **119**, 161101 (2017).
 - [2] B. P. Abbott, R. Abbott, T. D. Abbott, S. Abraham, F. Acernese, K. Ackley, C. Adams, R. X. Adhikari, V. B. Adya, C. Affeldt, et al., *Astrophys. J. Lett.* **892**, L3 (2020).
 - [3] B. D. Metzger, *Living Reviews in Relativity* **23**, 1 (2019).
 - [4] B. P. Abbott, R. Abbott, T. D. Abbott, F. Acernese, K. Ackley, C. Adams, T. Adams, P. Addesso, R. X. Adhikari, V. B. Adya, et al., *Astrophys. J. Lett.* **848**, L12 (2017).
 - [5] M. Shibata, *Phys. Rev. Lett.* **94**, 201101 (2005).
 - [6] L. Baiotti, B. Giacomazzo, and L. Rezzolla, *Phys. Rev. D* **78**, 084033 (2008).
 - [7] K. Hotokezaka, K. Kyutoku, H. Okawa, M. Shibata, and K. Kiuchi, *Phys. Rev. D* **83**, 124008 (2011).
 - [8] A. Bauswein, T. W. Baumgarte, and H.-T. Janka, *Phys. Rev. Lett.* **111**, 131101 (2013).
 - [9] J. A. Faber and F. A. Rasio, *Living Reviews in Relativity* **15**, 8 (2012).
 - [10] L. Baiotti and L. Rezzolla, *Reports on Progress in Physics* **80**, 096901 (2017).
 - [11] V. Paschalidis and N. Stergioulas, *Living Reviews in Relativity*

- ativity **20**, 7 (2017).
- [12] J. L. Friedman, International Journal of Modern Physics D **27**, 1843018 (2018).
- [13] A. Bauswein and N. Stergioulas, Journal of Physics G Nuclear Physics **46**, 113002 (2019).
- [14] L. Baiotti, Progress in Particle and Nuclear Physics **109**, 103714 (2019).
- [15] M. D. Duez and Y. Zlochower, Reports on Progress in Physics **82**, 016902 (2019).
- [16] M. Lucca and L. Sagunski, Journal of High Energy Astrophysics **27**, 33 (2020).
- [17] D. Radice, S. Bernuzzi, and A. Perego, Annual Review of Nuclear and Particle Science **70**, annurev (2020).
- [18] B. P. Abbott, R. Abbott, T. D. Abbott, F. Acernese, K. Ackley, C. Adams, T. Adams, P. Addesso, R. X. Adhikari, V. B. Adya, et al., Phys. Rev. X **9**, 011001 (2019).
- [19] J. Clark, A. Bauswein, L. Cadonati, H.-T. Janka, C. Pankow, and N. Stergioulas, Phys. Rev. D **90**, 062004 (2014).
- [20] A. Torres-Rivas, K. Chatziioannou, A. Bauswein, and J. A. Clark, Phys. Rev. D **99**, 044014 (2019).
- [21] A. Bauswein, S. Goriely, and H.-T. Janka, Astrophys. J. **773**, 78 (2013).
- [22] K. Hotokezaka, K. Kiuchi, K. Kyutoku, H. Okawa, Y.-i. Sekiguchi, M. Shibata, and K. Taniguchi, Phys. Rev. D **87**, 024001 (2013).
- [23] B. Margalit and B. D. Metzger, Astrophys. J. Lett. **880**, L15 (2019).
- [24] B. D. Metzger, ArXiv e-prints arXiv:1710.05931 (2017).
- [25] M. Ruiz and S. L. Shapiro, Phys. Rev. D **96**, 084063 (2017).
- [26] M. W. Coughlin, T. Dietrich, B. Margalit, and B. D. Metzger, Mon. Not. Roy. Astron. Soc. **489**, L91 (2019).
- [27] V. Paschalidis and M. Ruiz, Phys. Rev. D **100**, 043001 (2019).
- [28] H.-J. Lü, J. Shen, L. Lan, J. Rice, W.-H. Lei, and E.-W. Liang, Mon. Not. Roy. Astron. Soc. **486**, 4479 (2019).
- [29] R. Gill, A. Nathanail, and L. Rezzolla, Astrophys. J. **876**, 139 (2019).
- [30] R. J. Foley, D. A. Coulter, C. D. Kilpatrick, A. L. Piro, E. Ramirez-Ruiz, and J. Schwab, Mon. Not. Roy. Astron. Soc. (2020).
- [31] M. W. Coughlin, T. Dietrich, S. Antier, M. Bulla, F. Foucart, K. Hotokezaka, G. Raaijmakers, T. Hinderer, and S. Nissanke, Mon. Not. Roy. Astron. Soc. **492**, 863 (2020).
- [32] M. Agathos, F. Zappa, S. Bernuzzi, A. Perego, M. Breschi, and D. Radice, Phys. Rev. D **101**, 044006 (2020).
- [33] A. Chen, N. K. Johnson-McDaniel, T. Dietrich, and R. Dudi, Phys. Rev. D **101**, 103008 (2020).
- [34] C. J. Krüger and F. Foucart, Phys. Rev. D **101**, 103002 (2020).
- [35] S. Antier, S. Agayeva, V. Aivazyan, S. Alishov, E. Arbouch, A. Baransky, K. Barynova, J. M. Bai, S. Basa, S. Beradze, et al., Mon. Not. Roy. Astron. Soc. **492**, 3904 (2020).
- [36] A. Nathanail, Astrophys. J. **892**, 35 (2020).
- [37] A. Bauswein, O. Just, H.-T. Janka, and N. Stergioulas, Astrophys. J. Lett. **850**, L34 (2017).
- [38] S. Köppel, L. Bovard, and L. Rezzolla, Astrophys. J. Lett. **872**, L16 (2019).
- [39] C. D. Capano, I. Tews, S. M. Brown, B. Margalit, S. De, S. Kumar, D. A. Brown, B. Krishnan, and S. Reddy, Nature Astronomy (2020).
- [40] D. Radice, A. Perego, F. Zappa, and S. Bernuzzi, Astrophys. J. Lett. **852**, L29 (2018).
- [41] D. Radice and L. Dai, European Physical Journal A **55**, 50 (2019).
- [42] A. Bauswein, N.-U. F. Bastian, D. Blaschke, K. Chatziioannou, J. A. Clark, T. Fischer, H.-T. Janka, O. Just, M. Oertel, and N. Stergioulas, in *American Institute of Physics Conference Series* (2019), vol. 2127 of *American Institute of Physics Conference Series*, p. 020013.
- [43] J. Antoniadis, P. C. C. Freire, N. Wex, T. M. Tauris, R. S. Lynch, M. H. van Kerkwijk, M. Kramer, C. Bassa, V. S. Dhillon, T. Driebe, et al., Science **340**, 448 (2013).
- [44] Z. Arzoumanian, A. Brazier, S. Burke-Spolaor, S. Chamberlain, S. Chatterjee, B. Christy, J. M. Cordes, N. J. Cornish, F. Crawford, H. Thankful Cromartie, et al., Astrophys. J. Supp. **235**, 37 (2018).
- [45] H. T. Cromartie et al., Nat. Astron. **4**, 72 (2019).
- [46] P. D. Lasky, B. Haskell, V. Ravi, E. J. Howell, and D. M. Coward, Phys. Rev. D **89**, 047302 (2014).
- [47] S. Lawrence, J. G. Tervala, P. F. Bedaque, and M. C. Miller, Astrophys. J. **808**, 186 (2015).
- [48] C. L. Fryer, K. Belczynski, E. Ramirez-Ruiz, S. Rosswog, G. Shen, and A. W. Steiner, Astrophys. J. **812**, 24 (2015).
- [49] B. Margalit and B. D. Metzger, Astrophys. J. Lett. **850**, L19 (2017).
- [50] M. Shibata, S. Fujibayashi, K. Hotokezaka, K. Kiuchi, K. Kyutoku, Y. Sekiguchi, and M. Tanaka, Phys. Rev. D **96**, 123012 (2017).
- [51] L. Rezzolla, E. R. Most, and L. R. Weih, Astrophys. J. Lett. **852**, L25 (2018).
- [52] M. Ruiz, S. L. Shapiro, and A. Tsokaros, Phys. Rev. D **97**, 021501 (2018).
- [53] S. Ai, H. Gao, and B. Zhang, Astrophys. J. **893**, 146 (2020).
- [54] M. C. Miller, C. Chirenti, and F. K. Lamb, Astrophys. J. **888**, 12 (2020).
- [55] D.-S. Shao, S.-P. Tang, X. Sheng, J.-L. Jiang, Y.-Z. Wang, Z.-P. Jin, Y.-Z. Fan, and D.-M. Wei, Phys. Rev. D **101**, 063029 (2020).
- [56] F. Özel and P. Freire, Annual Review of Astronomy and Astrophysics **54**, 401 (2016).
- [57] J. M. Lattimer and M. Prakash, Physics Reports **621**, 127 (2016).
- [58] M. Oertel, M. Hempel, T. Klähn, and S. Typel, Reviews of Modern Physics **89**, 015007 (2017).
- [59] K. Sumiyoshi, S. Yamada, H. Suzuki, and S. Chiba, Phys. Rev. Lett. **97**, 091101 (2006).
- [60] T. Fischer, S. C. Whitehouse, A. Mezzacappa, F. K. Thielemann, and M. Liebendörfer, Astron. Astrophys. **499**, 1 (2009).
- [61] E. O'Connor and C. D. Ott, Astrophys. J. **730**, 70 (2011).
- [62] A. W. Steiner, M. Hempel, and T. Fischer, Astrophys. J. **774**, 17 (2013).
- [63] T. Fischer, M. Hempel, I. Sagert, Y. Suwa, and J. Schaffner-Bielich, European Physical Journal A **50**, 46 (2014).
- [64] A. d. S. Schneider, E. O'Connor, E. Granqvist, A. Betranhandy, and S. M. Couch, Astrophys. J. **894**, 4 (2020).
- [65] R. Oechslin, K. Uryū, G. Poghosyan, and F. K. Thiele-

- mann, Mon. Not. Roy. Astron. Soc. **349**, 1469 (2004).
- [66] V. Paschalidis, K. Yagi, D. Alvarez-Castillo, D. B. Blaschke, and A. Sedrakian, Phys. Rev. D **97**, 084038 (2018).
- [67] E. R. Most, L. J. Papenfort, V. Dexheimer, M. Hanauske, S. Schramm, H. Stöcker, and L. Rezzolla, Phys. Rev. Lett. **122**, 061101 (2019).
- [68] A. Bauswein, N.-U. F. Bastian, D. B. Blaschke, K. Chatziioannou, J. A. Clark, T. Fischer, and M. Oertel, Phys. Rev. Lett. **122**, 061102 (2019).
- [69] S. Han, M. A. A. Mamun, S. Lalit, C. Constantinou, and M. Prakash, Phys. Rev. D **100**, 103022 (2019).
- [70] J.-E. Christian, A. Zacchi, and J. Schaffner-Bielich, Phys. Rev. D **99**, 023009 (2019).
- [71] M. Sieniawska, W. Turczański, M. Bejger, and J. L. Zdunik, Astron. Astrophys. **622**, A174 (2019).
- [72] G. F. Burgio, A. Drago, G. Pagliara, H.-J. Schulze, and J.-B. Wei, Astrophys. J. **860**, 139 (2018).
- [73] A. Drago and G. Pagliara, Astrophys. J. Lett. **852**, L32 (2018).
- [74] V. Dexheimer, L. T. T. Soethe, J. Roark, R. O. Gomes, S. O. Kepler, and S. Schramm, arXiv e-prints arXiv:1901.03252 (2019).
- [75] K. Chatziioannou and S. Han, Phys. Rev. D **101**, 044019 (2020).
- [76] H.-Y. Chen, P. M. Chesler, and A. Loeb, Astrophys. J. Lett. **893**, L4 (2020).
- [77] M. G. Alford, S. Han, and K. Schwenzer, Journal of Physics G Nuclear Physics **46**, 114001 (2019).
- [78] R. De Pietri, A. Drago, A. Feo, G. Pagliara, M. Pasquali, S. Traversi, and G. Wiktorowicz, Astrophys. J. **881**, 122 (2019).
- [79] L. R. Weih, M. Hanauske, and L. Rezzolla, Phys. Rev. Lett. **124**, 171103 (2020).
- [80] M. G. Orsaria, G. Malfatti, M. Mariani, I. F. Ranea-Sandoval, F. García, W. M. Spinella, G. A. Contrera, G. Lugones, and F. Weber, Journal of Physics G Nuclear Physics **46**, 073002 (2019).
- [81] G. Montaña, L. Tolós, M. Hanauske, and L. Rezzolla, Phys. Rev. D **99**, 103009 (2019).
- [82] S. Han and A. W. Steiner, Phys. Rev. D **99**, 083014 (2019).
- [83] D. E. Alvarez-Castillo, D. B. Blaschke, A. G. Grunfeld, and V. P. Pagura, Phys. Rev. D **99**, 063010 (2019).
- [84] J. J. Li, A. Sedrakian, and M. Alford, Phys. Rev. D **101**, 063022 (2020).
- [85] J. P. Pereira, M. Bejger, N. Andersson, and F. Gittins, Astrophys. J. **895**, 28 (2020).
- [86] S. Blacker, N.-U. F. Bastian, A. Bauswein, D. B. Blaschke, T. Fischer, M. Oertel, T. Soutanis, and S. Typel, arXiv e-prints arXiv:2006.03789 (2020).
- [87] A. Bazavov, T. Bhattacharya, C. DeTar, H.-T. Ding, S. Gottlieb, R. Gupta, P. Hegde, U. M. Heller, F. Karsch, E. Laermann, et al., Phys. Rev. D **90**, 094503 (2014).
- [88] S. Borsányi, Z. Fodor, C. Hoelbling, S. D. Katz, S. Krieg, and K. K. Szabó, Physics Letters B **730**, 99 (2014).
- [89] B. Friman, C. Höhne, J. Knoll, S. Leupold, J. Randrup, R. Rapp, and P. Senger, eds., *The CBM Physics Book*, vol. 814 of *Lecture Notes in Physics*, Berlin Springer Verlag (2011).
- [90] D. Blaschke, J. Aichelin, E. Bratkovskaya, V. Friese, M. Gazdzicki, J. Randrup, O. Rogachevsky, O. Teryaev, and V. Toneev, European Physical Journal A **52**, 267 (2016).
- [91] J. Adamczewski-Musch et al. (HADES), Nature Phys. **15**, 1040 (2019).
- [92] B. P. Abbott, R. Abbott, T. D. Abbott, F. Acernese, K. Ackley, C. Adams, T. Adams, P. Addesso, R. X. Adhikari, V. B. Adya, et al., Astrophys. J. Lett. **851**, L16 (2017).
- [93] R. Dudi, F. Pannarale, T. Dietrich, M. Hannam, S. Bernuzzi, F. Ohme, and B. Brügmann, Phys. Rev. D **98**, 084061 (2018).
- [94] H. Yang, V. Paschalidis, K. Yagi, L. Lehner, F. Pretorius, and N. Yunes, Phys. Rev. D **97**, 024049 (2018).
- [95] K. W. Tsang, T. Dietrich, and C. Van Den Broeck, Phys. Rev. D **100**, 044047 (2019).
- [96] M. Breschi, S. Bernuzzi, F. Zappa, M. Agathos, A. Perego, D. Radice, and A. Nagar, Phys. Rev. D **100**, 104029 (2019).
- [97] J. Isenberg and J. Nester, in *General Relativity and Gravitation. Vol. 1. One hundred years after the birth of Albert Einstein*. Edited by A. Held. New York, NY: Plenum Press, p. 23, 1980, edited by A. Held (1980), p. 23.
- [98] J. R. Wilson, G. J. Mathews, and P. Marronetti, Phys. Rev. D **54**, 1317 (1996).
- [99] R. Oechslin, S. Rosswog, and F.-K. Thielemann, Phys. Rev. D **65**, 103005 (2002).
- [100] R. Oechslin, H.-T. Janka, and A. Marek, Astron. Astrophys. **467**, 395 (2007).
- [101] A. Bauswein, H.-T. Janka, and R. Oechslin, Phys. Rev. D **82**, 084043 (2010).
- [102] A. Bauswein, H.-T. Janka, K. Hebeler, and A. Schwenk, Phys. Rev. D **86**, 063001 (2012).
- [103] A. Bauswein, N. Stergioulas, and H.-T. Janka, Phys. Rev. D **90**, 023002 (2014).
- [104] A. Bauswein and et al., in preparation, to be submitted to Phys. Rev. D (2020).
- [105] S. Banik, M. Hempel, and D. Bandyopadhyay, Astrophys. J. Supp. **214**, 22 (2014).
- [106] M. Fortin, M. Oertel, and C. Providência, Publications of the Astronomical Society of Australia **35** (2018).
- [107] M. Marques, M. Oertel, M. Hempel, and J. Novak, Phys. Rev. **C96**, 045806 (2017).
- [108] M. Hempel and J. Schaffner-Bielich, Nucl. Phys. A **837**, 210 (2010).
- [109] S. Typel, G. Röpke, T. Klähn, D. Blaschke, and H. H. Wolter, Phys. Rev. C **81**, 015803 (2010).
- [110] S. Typel, Phys. Rev. C **71**, 064301 (2005).
- [111] D. Alvarez-Castillo, A. Ayriyan, S. Benic, D. Blaschke, H. Grigorian, and S. Typel, European Physical Journal A **52**, 69 (2016).
- [112] A. Akmal, V. R. Pandharipande, and D. G. Ravenhall, Phys. Rev. C **58**, 1804 (1998).
- [113] S. Goriely, N. Chamel, and J. M. Pearson, Phys. Rev. C **82**, 035804 (2010).
- [114] R. B. Wiringa, V. Fiks, and A. Fabrocini, Phys. Rev. C **38**, 1010 (1988).
- [115] J. M. Lattimer and F. Douglas Swesty, Nuclear Physics A **535**, 331 (1991).
- [116] G. Shen, C. J. Horowitz, and S. Teige, Phys. Rev. C **83**, 035802 (2011).
- [117] G. A. Lalazissis, J. König, and P. Ring, Phys. Rev. C **55**, 540 (1997).
- [118] M. Hempel, T. Fischer, J. Schaffner-Bielich, and M. Liebendörfer, Astrophys. J. **748**, 70 (2012).
- [119] F. Douchin and P. Haensel, Astron. Astrophys. **380**, 151 (2001).

- [120] H. M \ddot{u} ther, M. Prakash, and T. L. Ainsworth, *Physics Letters B* **199**, 469 (1987).
- [121] M. Alford, M. Braby, M. Paris, and S. Reddy, *Astrophys. J.* **629**, 969 (2005).
- [122] L. Engvik, E. Osnes, M. Hjorth-Jensen, G. Bao, and E. Ostgaard, *Astrophys. J.* **469**, 794 (1996).
- [123] A. S. Schneider, C. Constantinou, B. Muccioli, and M. Prakash, *Phys. Rev. C* **100**, 025803 (2019).
- [124] J. S. Read, B. D. Lackey, B. J. Owen, and J. L. Friedman, *Phys. Rev. D* **79**, 124032 (2009).
- [125] B. D. Lackey, M. Nayyar, and B. J. Owen, *Phys. Rev. D* **73**, 024021 (2006).
- [126] N. K. Glendenning, *Astrophys. J.* **293**, 470 (1985).
- [127] Y. Sugahara and H. Toki, *Nuclear Physics A* **579**, 557 (1994).
- [128] H. Toki, D. Hirata, Y. Sugahara, K. Sumiyoshi, and I. Tanihata, *Nuclear Physics A* **588**, 357 (1995).
- [129] M. A. R. Kaltenborn, N.-U. F. Bastian, and D. B. Blaschke, *Phys. Rev. D* **96**, 056024 (2017).
- [130] N.-U. Bastian, D. Blaschke, T. Fischer, and G. R \ddot{o} pke, *Universe* **4**, 67 (2018).
- [131] M. Cierniak, T. Kl \ddot{a} hn, T. Fischer, and N.-U. Bastian, *Universe* **4**, 30 (2018), 1802.03214.
- [132] T. Fischer, N.-U. F. Bastian, M.-R. Wu, P. Baklanov, E. Sorokina, S. Blinnikov, S. Typel, T. Kl \ddot{a} hn, and D. B. Blaschke, *Nature Astronomy* **2**, 980 (2018).
- [133] T. Kl \ddot{a} hn and T. Fischer, *Astrophys. J.* **810**, 134 (2015).
- [134] Y. Nambu and G. Jona-Lasinio, *Phys. Rev.* **122**, 345 (1961).
- [135] S. Klevansky, *Rev. Mod. Phys.* **64**, 649 (1992).
- [136] T. Kl \ddot{a} hn, T. Fischer, and M. Hempel, *Astrophys. J.* **836**, 89 (2017).
- [137] D. S. Balsara, *Journal of Computational Physics* **121**, 357 (1995).
- [138] J. S. Read, C. Markakis, M. Shibata, K. Ury \ddot{u} , J. D. E. Creighton, and J. L. Friedman, *Phys. Rev. D* **79**, 124033 (2009).
- [139] W. Del Pozzo, T. G. F. Li, M. Agathos, C. Van Den Broeck, and S. Vitale, *Phys. Rev. Lett.* **111**, 071101 (2013).
- [140] J. S. Read, L. Baiotti, J. D. E. Creighton, J. L. Friedman, B. Giacomazzo, K. Kyutoku, C. Markakis, L. Rezzolla, M. Shibata, and K. Taniguchi, *Phys. Rev. D* **88**, 044042 (2013).
- [141] L. Wade, J. D. E. Creighton, E. Ochsner, B. D. Lackey, B. F. Farr, T. B. Littenberg, and V. Raymond, *Phys. Rev. D* **89**, 103012 (2014).
- [142] M. Agathos, J. Meidam, W. Del Pozzo, T. G. F. Li, M. Tompitak, J. Veitch, S. Vitale, and C. Van Den Broeck, *Phys. Rev. D* **92**, 023012 (2015).
- [143] K. Chatziioannou, K. Yagi, A. Klein, N. Cornish, and N. Yunes, *Phys. Rev. D* **92**, 104008 (2015).
- [144] K. Hotokezaka, K. Kyutoku, Y.-i. Sekiguchi, and M. Shibata, *Phys. Rev. D* **93**, 064082 (2016).
- [145] K. Chatziioannou, C.-J. Haster, and A. Zimmerman, *Phys. Rev. D* **97**, 104036 (2018).
- [146] S. De, D. Finstad, J. M. Lattimer, D. A. Brown, E. Berger, and C. M. Biwer, *Phys. Rev. Lett.* **121**, 091102 (2018).
- [147] T. Hinderer, *Astrophys. J.* **677**, 1216 (2008).
- [148] T. Hinderer, B. D. Lackey, R. N. Lang, and J. S. Read, *Phys. Rev. D* **81**, 123016 (2010).
- [149] T. Damour and A. Nagar, *Phys. Rev. D* **81**, 084016 (2010).
- [150] M. C. Miller, F. K. Lamb, A. J. Dittmann, S. Bogdanov, Z. Arzoumanian, K. C. Gendreau, S. Guillot, A. K. Harding, W. C. G. Ho, J. M. Lattimer, et al., *Astrophys. J. Lett.* **887**, L24 (2019).
- [151] T. E. Riley, A. L. Watts, S. Bogdanov, P. S. Ray, R. M. Ludlam, S. Guillot, Z. Arzoumanian, C. L. Baker, A. V. Bilous, D. Chakrabarty, et al., *Astrophys. J. Lett.* **887**, L21 (2019).
- [152] G. Raaijmakers, S. K. Greif, T. E. Riley, T. Hinderer, K. Hebeler, A. Schwenk, A. L. Watts, S. Nissanke, S. Guillot, J. M. Lattimer, et al., *Astrophys. J. Lett.* **893**, L21 (2020).
- [153] A. Bauswein and N. Stergioulas, *Mon. Not. Roy. Astron. Soc.* **471**, 4956 (2017).
- [154] F. Zappa, S. Bernuzzi, D. Radice, A. Perego, and T. Dietrich, *Phys. Rev. Lett.* **120**, 111101 (2018).
- [155] S. Bernuzzi, M. Breschi, B. Daszuta, A. Endrizzi, D. Logoteta, V. Nedora, A. Perego, D. Radice, F. Schianchi, F. Zappa, et al., *Mon. Not. Roy. Astron. Soc.* **497**, 1488 (2020).
- [156] K. Kiuchi, K. Kyutoku, M. Shibata, and K. Taniguchi, *Astrophys. J. Lett.* **876**, L31 (2019).
- [157] P. Danielewicz, R. Lacey, and W. G. Lynch, *Science* **298**, 1592 (2002).
- [158] C. Y. Tsang, M. B. Tsang, P. Danielewicz, W. G. Lynch, and F. J. Fattoyev, *ArXiv e-prints* (2018), 1807.06571.
- [159] J. M. Lattimer and Y. Lim, *Astrophys. J.* **771**, 51 (2013).
- [160] T. Kr \ddot{u} ger, I. Tews, K. Hebeler, and A. Schwenk, *Phys. Rev. C* **88**, 025802 (2013).
- [161] B. P. Abbott, R. Abbott, T. D. Abbott, F. Acernese, K. Ackley, C. Adams, T. Adams, P. Addesso, R. X. Adhikari, V. B. Adya, et al., *Phys. Rev. Lett.* **121**, 161101 (2018).

Supplemental Material

EQUATION OF STATE SAMPLE, SIMULATIONS AND FIT FORMULAE

In this letter, we describe the collapse behavior, i.e. the threshold mass for prompt BH formation, for a large sample of EoS models. We perform three-dimensional relativistic hydrodynamical simulations as in [1–5] to determine M_{thres} . All these simulations make the following assumptions about the initial data. The NSs have an irrotational velocity field, i.e. no intrinsic spin, and the stellar matter is at zero temperature. The composition (electron fraction) is given by neutrino-less beta-equilibrium. We start calculations a few cycles before merging and assume a quasi-circular orbit. We explicitly refer to these earlier publications for more details and additional information.

By considering calculations with different M_{tot} and determining the respective merger product, we obtain M_{thres} with an accuracy of at least $\pm 0.025 M_{\odot}$. For every EoS we vary M_{tot} in steps of $0.05 M_{\odot}$ and define the threshold mass as $M_{\text{thres}} = 0.5(M_{\text{tot,delayed}} + M_{\text{tot,prompt}})$. Within our set of simulations $M_{\text{tot,delayed}}$ ($M_{\text{tot,prompt}}$) is the binary mass of the most (least) massive system leading to a delayed (prompt) collapse. (We define a prompt-collapse event as those systems where the minimum lapse function α_{min} continuously decreases and never increases after merging. This is a meaningful definition because an increasing α_{min} implies a bounce of the merging binary components, which leads to an increase of the ejecta mass and thus to a fundamentally different electromagnetic signal compared to a prompt collapse.) We follow this prescription to determine M_{thres} for fixed mass ratios of $q = M_1/M_2 = 0.7$ and $q = 1$.

In total we consider 40 EoS models (see Tab. I), which we group in three subsets:

(a) The “base sample” consists of 23 purely hadronic EoSs which are compatible with current astrophysical constraints from pulsar mass measurements and from limits on the tidal deformability in GW170817. We require the maximum mass of nonrotating NSs to be larger than $1.97 M_{\odot}$, which is the lower bound of the error bars from [6, 7], and we require the tidal deformability of a $1.37 M_{\odot}$ NS to be smaller than 800, which is the less stringent limit from an analysis of finite-size effects during the inspiral of GW170817 [8]. Generally, we prefer to be less restrictive with regard to possible constraints to include as many models as possible for a sufficient coverage of the parameter space.

(b) An extended hadronic sample includes additional 8 hadronic models which are incompatible with the aforementioned measurements (at the two sigma and 90% confidence level, respectively). We refer to this set as “ex-

cluded hadronic sample” which is useful to cover even more models and understand dependencies.

(c) The “hybrid sample” comprises a set of 9 different EoSs which feature a phase transition to deconfined quark matter beyond some transition density [9]. This sample serves to investigate the impact of a phase transition on the threshold binary mass for prompt collapse. Most of these models have been employed in [10], where additional information can be found³. These models are based on a single hadronic EoS below the transition density, but differ in the properties of the quark matter phase. This leads to different onset densities of the phase transition, different latent heat (density jump across the phase transition) and different stiffness of the quark phase EoS. All hybrid models are fully temperature dependent. This is important because also the phase boundaries vary with temperature, which cannot be easily captured by a simplified treatment of thermal effects (see e.g. [3]).

Note that sample (a) includes the ALF2 EoS implemented as piecewise polytrope [33, 35]. This EoS is formally a hybrid model with a transition to quark matter. However, it is build such that it resembles the properties of hadronic matter, which is why we count it for the hadronic sample. The base sample contains three EoSs with a transition to hyperonic matter, and the excluded hadronic sample includes another two of such models.

All EoS models are listed in Tab. I, which includes the references for each EoS. We indicate in Tab. I to which subset a given EoS model belongs. The table also includes different stellar parameters, which we employ to characterize the EoSs: the maximum mass M_{max} of a nonrotating NS, the radius of a nonrotating NS with $1.6 M_{\odot}$ and the tidal deformability of a $1.4 M_{\odot}$ NS.

26 EoSs of our total sample are implemented in the form of tables, which include the temperature and com-

³ One of the models within our hybrid sample has not been described previously. The vector-interaction enhanced bag model (vBAG) has been derived from the Schwinger-Dyson formalism of QCD as limiting case for a particular choice of the gluon propagator (for details see Ref. [11]). VBAG features chiral symmetry restoration via a chiral bag constant, in which aspect vBAG resembles thermodynamic results of commonly used EoSs of the Nambu-Jona-Lasinio type [12, 13]. Furthermore, (de)confinement is taken into account through an additional bag constant which is directly linked to properties of the underlying hadronic EOS [14–16] at the chiral symmetry restoration. This approach ensures the simultaneous restoration of chiral symmetry and (de)confinement [17]. Also, one model of the DD2F-SF family of hybrid EoSs (DD2F-SF8) was not included in [10], which is why we here provide its specific parameters, namely $\sqrt{D_0} = 240 \text{ MeV}$, $\alpha = 0.1 \text{ fm}^6$, $a = 0.0 \text{ MeV fm}^3$, $b = 0.0 \text{ MeV fm}^9$, $c = 0.0 \text{ fm}^6$, $\rho_1 = 80 \text{ MeV fm}^3$ (see [10, 38]).

EoS	T/B	M_{\max} (M_{\odot})	$R_{1.6}$ (km)	$\Lambda_{1.4}$	$M_{\text{thres}}(q=1)$ (M_{\odot})	$\tilde{\Lambda}_{\text{thres}}(q=1)$	$M_{\text{thres}}(q=0.7)$ (M_{\odot})	$\tilde{\Lambda}_{\text{thres}}(q=0.7)$	sample	Ref.
BHBLP	T	2.098	13.192	691.0	3.125	353.8	2.975	512.8	b	[18]
DD2Y	T	2.031	13.169	691.0	3.075	389.2	2.875	622.1	b	[19, 20]
DD2	T	2.419	13.247	694.8	3.325	248.0	3.275	300.3	b	[14, 15]
DD2F	T	2.077	12.220	423.1	2.925	315.0	2.850	427.7	b	[15, 21, 22]
APR	B	2.187	11.253	245.9	2.825	232.2	2.825	260.2	b	[23]
BSK20	B	2.165	11.648	317.4	2.875	267.6	2.875	300.3	b	[24]
eosUU	B	2.189	11.057	227.9	2.825	215.2	2.825	241.1	b	[25]
LS220	T	2.041	12.478	537.0	2.975	350.6	2.875	519.0	b	[26]
LS375	T	2.709	13.767	950.8	3.575	223.5	3.575	248.5	e	[26]
GS2	T	2.089	13.369	717.2	3.175	322.7	3.025	487.3	e	[27]
NL3	T	2.787	14.795	1360.3	3.775	228.5	3.775	257.9	e	[14, 28]
Sly4	B	2.043	11.523	292.4	2.825	275.4	2.775	352.8	b	[29]
SFHO	T	2.056	11.751	331.5	2.875	278.2	2.825	352.9	b	[30]
SFHOY	T	1.986	11.748	331.5	2.825	312.6	2.725	441.5	b	[19, 20]
SFHX	T	2.127	11.963	393.1	2.975	269.3	2.925	328.3	b	[30]
TM1	T	2.210	14.347	1142.0	3.375	334.5	3.225	525.0	e	[16, 31]
TMA	T	2.008	13.660	928.0	3.175	396.9	2.975	698.1	e	[16, 32]
BSK21	B	2.276	12.543	511.4	3.075	287.1	3.075	317.7	b	[24]
GS1	T	2.750	14.864	1392.1	3.775	229.6	3.775	260.4	e	[27]
eosAU	B	2.125	10.357	149.9	2.675	200.3	2.675	222.2	b	[25]
WFF1	B	2.118	10.362	150.0	2.675	200.2	2.675	220.1	b	[25, 33]
WFF2	B	2.186	11.048	222.4	2.825	210.0	2.825	235.3	b	[25, 33]
MPA1	B	2.454	12.448	475.9	3.225	202.2	3.225	224.6	b	[33, 34]
ALF2	B	1.973	12.616	565.1	2.975	385.2	2.875	510.1	b	[33, 35]
H4	B	2.010	13.716	846.4	3.125	403.6	2.925	699.6	e	[33, 36]
DD2F-SF-1	T	2.134	12.141	423.1	2.845	380.4	2.770	497.8	h	[9, 10, 37, 38]
DD2F-SF-2	T	2.160	12.061	421.2	2.925	298.6	2.870	399.3	h	[9, 10, 37, 38]
DD2F-SF-3	T	2.032	12.189	423.1	2.825	398.8	2.720	570.1	h	[9, 10, 37, 38]
DD2F-SF-4	T	2.029	12.220	423.1	2.835	389.5	2.725	566.9	h	[9, 10, 37, 38]
DD2F-SF-5	T	2.038	11.928	423.1	2.815	408.4	2.725	539.2	h	[9, 10, 37, 38]
DD2F-SF-6	T	2.012	12.219	423.1	2.795	428.1	2.675	635.5	h	[9, 10, 37, 38]
DD2F-SF-7	T	2.115	12.220	423.1	2.905	330.2	2.825	451.2	h	[9, 10, 37, 38]
DD2F-SF-8	T	2.025	12.216	422.3	2.915	321.9	2.810	467.3	h	[9, 10, 37, 38]
VBAG	T	1.932	12.214	422.3	2.885	345.5	2.775	505.4	h	[39]
ENG	B	2.236	11.899	367.5	2.975	249.3	2.975	279.7	b	[33, 40]
APR3	B	2.363	11.954	364.8	3.075	204.6	3.075	228.1	b	[23, 33]
GNH3	B	1.959	13.756	850.4	3.075	432.6	2.875	799.3	e	[33, 41]
SAPR	T	2.194	11.462	265.7	2.875	223.7	2.875	254.5	b	[42]
SAPRLDP	T	2.247	12.369	449.3	3.025	271.0	3.025	309.4	b	[42]
SSkAPR	T	2.028	12.304	442.6	2.950	312.7	2.875	420.8	b	[42]

TABLE I: EoS employed in this study. Second column indicates whether EoS table provides temperature dependence (T) or whether table is barotropic and supplemented by an approximate temperature treatment (B). Next three columns list stellar parameters which characterize the EoS, i.e. maximum mass M_{\max} , radius $R_{1.6}$ of a $1.6 M_{\odot}$ NS and tidal deformability of a $1.4 M_{\odot}$ NS. Next four columns provide threshold binary mass M_{thres} for prompt collapse and combined tidal deformability at M_{thres} for equal-mass mergers and asymmetric mergers with a binary mass ratio $q = 0.7$. Penultimate entry classifies to which of the three EoS samples the given model belongs, where “b” stands for “base sample”, “e” for “excluded hadronic sample” and “h” for “hybrid sample”. Last column gives reference of EoS model.

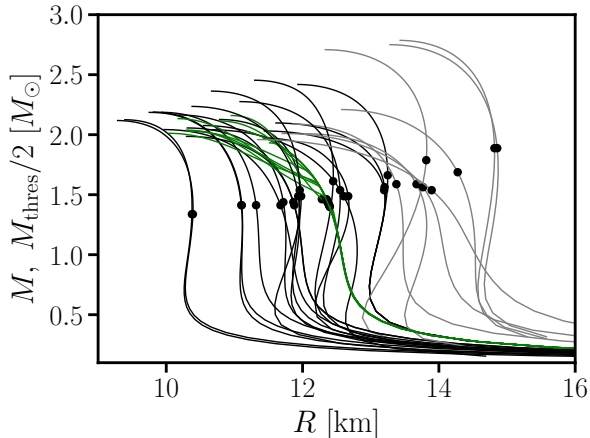


FIG. 1: Mass-radius relations for the EoS models employed in this study. Black lines display the purely hadronic base sample, while gray curves show purely hadronic EoSs which are incompatible with current astrophysical constraints. Models of the hybrid sample are plotted in green. The dots visualize $M_{\text{thres}}/2$ of the respective EoS. See main text for more explanations.

position dependence. For the remaining models, which provide the EoS only at $T = 0$, we use an approximate prescription of the thermal pressure, setting the tunable thermal ideal-gas index $\Gamma_{\text{th}} = 1.75$ (see [3]). The temperature dependent models are marked with a “T” in Tab. I, barotropic EoSs are indicated by “B”.

Figure 1 shows the resulting mass-radius relations for all EoSs employed in this study. The hadronic base sample is displayed by black lines and the excluded hadronic sample by gray lines. The green lines depict the hybrid models featuring a characteristic kink at M_{onset} , which is the smallest mass where quark matter is present (see also Fig. 2 in [10] for a zoom-in). Figure 1 demonstrates that our set of models covers the full viable range of hadronic EoSs with regard to the range of stellar parameters. This is crucial because in the main text we argue that hadronic models are constrained to a certain area in the $M_{\text{thres}} - \tilde{\Lambda}_{\text{thres}}$ plane, dubbed “mixed regime”. It is thus reasonable to expect that any other hadronic EoS will also follow this behavior. It should approximately resemble one of the EoSs from our sample which is the most similar one to it. Note that there is a unique relation between the M-R relations and the EoS for zero-temperature models. Hence, also the viable range of thermodynamical properties, explicitly $P(\rho)$ is well sampled by our set of EoS models.

As mentioned, the hybrid models in our sample employ a single hadronic model at lower densities. In this context we recall that this hadronic EoS is fully compatible with current astrophysical and nuclear physics constraints (see [6, 8, 43–51]). In fact, it roughly falls in the

middle of the ranges given by these measurements. We thus expect that variations to this model do not lead to a fundamentally different behavior.

The dots in Fig. 1 visualize the threshold mass for prompt BH formation for the different EoSs with a binary mass ratio $q = 1$. We plot $M_{\text{thres}}/2$ on the mass-radius relation of the corresponding EoS at $(R(M_{\text{thres}}/2), M_{\text{thres}}/2)$. The dots thus show the radii $R_{\text{thres}} = R(M_{\text{thres}}/2)$ of the inspiraling stars before merging. The figure illustrates that the radii $R_{1.6}$ of $1.6 M_{\odot}$ NSs are well suited to characterize the relevant EoS regime of binaries close to the threshold for prompt collapse. Note that densities increase during merging. Hence, the collapse behavior is also affected by the EoS at higher densities than those which are realized in stars with $M_{\text{thres}}/2$. This explains that the combination $R_{1.6}$ and M_{max} represents a good choice to characterize the collapse behavior.

Table I provides the threshold masses for equal-mass binaries and for asymmetric binaries with a mass ratio $q = 0.7$. In addition, we list $\tilde{\Lambda}_{\text{thres}}$ as the combined tidal deformability of the binary with the threshold mass for every EoS model and mass ratio considered in this study. Note that for equal-mass binaries $\tilde{\Lambda}_{\text{thres}} = \Lambda(M_{\text{thres}}/2)$.

Based on the data in Tab. I we construct different bilinear fit formulae describing the collapse behavior of NS mergers, which are discussed in the main paper. These relations connect M_{max} , M_{thres} and one more stellar parameter characterizing the EoS. We provide these relations in Tab. II with the maximum mass M_{max} being the dependent variable. We emphasize that these fits are bilinear. It is thus trivial to obtain relations with M_{thres} (or any other quantity) being the dependent variable, which may be useful for many applications (see main paper). The various choices for the fit functions and the underlying data set are motivated by different assumptions on which quantities may be measured or constrained. The quality of the relations is quantified by the maximum residual and the average deviation between fit and data.

Note that M_{thres} for some of the EoSs which have already been considered in [5] slightly differ from the values reported therein. The reasons are that here we determine M_{thres} with higher accuracy, i.e. finer sampling in M_{tot} , and we slightly modified the treatment of artificial viscosity within the smooth particle hydrodynamics scheme by implementing an additional factor for lowering viscosity in a pure shear flow [52].

We finally remark that the results presented in Tabs. I and II constitute the largest study of the collapse behavior of binary mergers to date. It includes the largest set of EoS models and it determines for the first time systematically the threshold mass for asymmetric mergers. In this study we intentionally do not include additional data from other groups, which are publicly available [53–56]. First, this would not enlarge our sample significantly. Second, for this study it is important to work with a con-

no.	fit	EoS sample	q	a	b	c	max. dev.	av. dev.
1	$M_{\max} = aM_{\text{thres}} + b\tilde{\Lambda}_{\text{thres}} + c$	base sample	1.0	0.632	-1.866e-03	0.802	0.067	0.023
1e	$M_{\max} = aM_{\text{thres}} + b\tilde{\Lambda}_{\text{thres}} + c$	base sample + 8 excl. had. ^a	1.0	0.63	-2.002e-03	0.841	0.106	0.031
2	$M_{\max} = aM_{\text{thres}} + b\tilde{\Lambda}_{\text{thres}} + c$	base sample	0.7	0.621	-6.637e-04	0.582	0.078	0.023
3	$M_{\max} = aM_{\text{thres}} + b\tilde{\Lambda}_{\text{thres}} + c$	base sample	1.0 and 0.7	0.53	-7.409e-04	0.833	0.153	0.051
4	$M_{\max} = aM_{\text{thres}} + b\tilde{\Lambda}_{\text{thres}} + c$	base sample + 9 hyb.	1.0	0.477	-1.156e-03	1.077	0.138	0.054
5	$M_{\max} = aM_{\text{thres}} + b\tilde{\Lambda}_{\text{thres}} + c$	base sample + 4 hyb. ^b	1.0	0.627	-1.840e-03	0.811	0.089	0.028
6	$M_{\max} = a\mathcal{M}_{c,\text{thres}} + b\tilde{\Lambda}_{\text{thres}} + c$	base sample	1.0 and 0.7	1.073	-6.956e-04	1.018	0.166	0.057
7	$M_{\max} = a\mathcal{M}_{c,\text{thres}} + b\tilde{\Lambda}_{\text{thres}} + c$	base sample + 9 hyp	1.0 and 0.7	0.899	-4.680e-04	1.167	0.203	0.066
8	$M_{\max} = aM_{\text{thres}} + b\Lambda_{1.4} + c$	base sample	1.0	1.47	-1.166e-03	-1.714	0.08	0.039
9	$M_{\max} = aM_{\text{thres}} + b\Lambda_{1.4} + c$	base sample	0.7	1.052	-5.709e-04	-0.671	0.072	0.03
10	$M_{\max} = aM_{\text{thres}} + bR_{1.6} + c$	base sample	1.0	1.685	-2.761e-01	0.488	0.078	0.029
11	$M_{\max} = aM_{\text{thres}} + bR_{1.6} + c$	base sample	0.7	1.143	-1.318e-01	0.412	0.07	0.021
12	$M_{\text{thres}}^{q=1} - M_{\text{thres}}^{q=0.7} = aM_{\max} + bR_{1.6} + c$	base sample	1.0 and 0.7	-0.285	4.859e-02	0.079	0.061	0.019

^aWe include 8 hadronic EoS incompatible with [8].

^bWe include hybrid models with $(M_{\text{thres}}, \tilde{\Lambda}_{\text{thres}})$ below the dashed line in Fig. 2 in the main paper.

TABLE II: Different bilinear fits describing the collapse behavior (see main text). Third and fourth columns list the data set employed for the fit specifying the sample of EoSs and the binary mass ratio q . a , b and c are fit parameters. Last two columns provide the maximum and average deviation between fit and the underlying data. All units are such that masses are in M_{\odot} and radii in km; Λ is dimensionless.

sistent set of data to quantify the quality of fit relations. Other studies determine M_{thres} with different accuracy and, moreover, it is difficult to assess intrinsic model dependencies of other simulation results like for instance the resolution dependence, EoS implementation or residual orbital eccentricity. Generally, there is a very good agreement comparing our results to the ones from other groups [53–56]. This said we stress that more future work will be required to fully understand the impact of the numerical treatment and different physical effects on M_{thres} . Clearly, our new findings highlight the scientific value of such future efforts.

IMPACT OF BINARY MASS RATIO

In this study we determine the threshold binary mass for fixed mass ratios of $q = 0.7$ and $q = 1$, which is the range inferred for GW170817. Since the sensitivity of current GW instruments continues to increase, future merger observations will reveal the binary mass with higher accuracy at the same distance, whereas the mass ratio of events at larger distance will not be obtained with good precision. Therefore, we construct fit formulae for fixed mass ratios as well as for a range of mass ratios.

Determining M_{thres} for a range in q is important for observations where the mass ratio is not known very well. Obviously, in simulations the threshold mass can only be computed for fixed mass ratios. Hence, the range of M_{thres} for $0.7 \leq q \leq 1$ is determined by individual models. We explicitly assume that M_{thres} varies monotonically

with q , such that $M_{\text{thres}}(q = 1)$ and $M_{\text{thres}}(q = 0.7)$ are sufficient to specify the range. While this is a very reasonable assumption and physically intuitive, we confirm this by additional calculations for selected EoS models.

Figure 2 shows $M_{\text{thres}}(q)$ for the DD2F and SFHX EoSs, where we explicitly calculate M_{thres} for $q = \{0.6, 0.7, 0.8, 0.9, 1.0\}$. The error bars specify the precision to which M_{thres} was determined in the simulations (with the upper edge being $M_{\text{tot,prompt}}$ and the lower edge being $M_{\text{tot,delayed}}$ as described above). Within the given accuracy the calculations confirm that $M_{\text{thres}}(q)$ is indeed a monotonic function of the mass ratio q . Note that the dependence on q is not precisely linear but follows approximately a higher-order polynomial. By a fit assuming a dependence $(1 - q)^n$ we determine a power of $n = 2.89$ for DD2F and $n = 3.53$ for SFHX. The impact of the mass ratio thus becomes stronger for stronger binary mass asymmetry. For small deviations from $q = 1$ the threshold mass is roughly constant. We find a qualitatively similar behavior in additional simulations for the DD2 and SAPR EoSs. Our observations are in line with previous calculations for $q = 0.9$ in [5] and for $q = 0.6$ in [49]. These conclusions are also consistent with the simulations for fixed mass in [57], which however do not directly determine M_{thres} .

Figure 2 and the data in Tab. I show a very clear dependence on the binary mass ratio, namely, generally, a decrease of M_{thres} with asymmetry. This general behavior is physically understandable based on Newtonian point particles. For the same total mass and the same

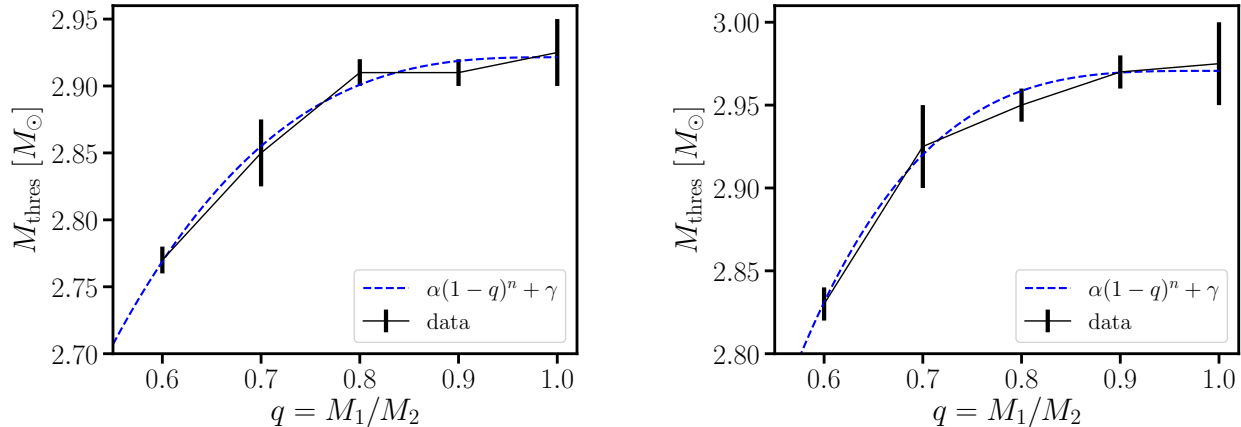


FIG. 2: Threshold binary mass for prompt BH formation as function of the binary mass ratio q for the DD2F EoS (left panel) and the SFHX EoS (right panel). The width of the error bar indicates the accuracy to which M_{thres} has been determined for the given q (see main text). The dashed blue curve shows a least-squares fit of the form $M_{\text{thres}}(q) = \alpha(1 - q)^n + \gamma$.

orbital distance, circular orbits of asymmetric binaries have less angular momentum than equal-mass systems. Hence, the available angular momentum to support the merger remnant is reduced for $q < 1$ leading to smaller M_{thres} (assuming the merging to take place at the same orbital distance).

We finally comment on a finding that we already highlight in the main paper. The impact of the mass ratio on M_{thres} is differently strong for different EoSs (see last fit in Tab. II). Importantly, also the difference between $M_{\text{thres}}(q = 1)$ and $M_{\text{thres}}(q = 0.7)$ follows a specific EoS dependence, which can be well described by $\Delta M_{\text{thres}} = M_{\text{thres}}(q = 1) - M_{\text{thres}}(q = 0.7) = aM_{\text{max}} + bR_{1.6} + c$ with the fit parameters given in Tab. II. Figure 3 shows this relation for ΔM_{thres} and demonstrates its tightness.

A more extended discussion of mass ratio effects on the collapse behavior will be presented in a forthcoming publication. Here we still note that this particular dependence of ΔM_{thres} also explains the findings of [58], which tentatively indicate that for soft EoSs which yield very small NS radii, the remnants of asymmetric mergers may be more stable than that of equal-mass binaries of the same total mass⁴. A stronger stabilization of remnants resulting from asymmetric mergers would seem somewhat in tension with the results from [5, 49, 57], which show a destabilization for stiffer EoS models if q deviates from unity. All these different findings however become fully consistent in the light of the particular EoS dependence revealed by Fig. 3. It clearly shows that for

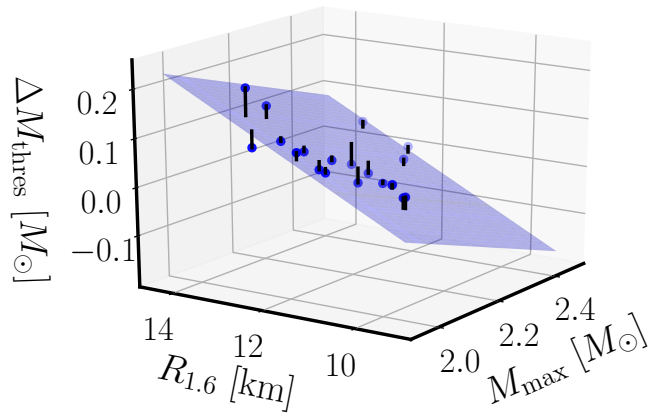


FIG. 3: Impact of the binary mass ratio on the collapse behavior of NS mergers for the hadronic base sample. Blue dots display ΔM_{thres} as the difference between the threshold mass for prompt collapse of equal-mass binaries and of asymmetric binaries with $q = 0.7$ as function of the maximum mass M_{max} and radius $R_{1.6}$ of $1.6 M_{\odot}$ NSs. The blue plane is a bilinear fit to the data. Short black lines visualize the deviations between fit and underlying data.

very soft EoSs $M_{\text{thres}}(q = 1)$ and $M_{\text{thres}}(q = 0.7)$ are very comparable and that the threshold mass for asymmetric mergers may even be larger than the one of equal-mass binaries in a small parameter range.

⁴ Note that [58] runs only simulations for a fixed total binary mass without determining M_{thres} .

-
- [1] R. Oechslin, S. Rosswog, and F.-K. Thielemann, Phys. Rev. D **65**, 103005 (2002).
 - [2] R. Oechslin, H.-T. Janka, and A. Marek, Astron. Astrophys. **467**, 395 (2007).
 - [3] A. Bauswein, H.-T. Janka, and R. Oechslin, Phys. Rev.

- D **82**, 084043 (2010).
- [4] A. Bauswein, H.-T. Janka, K. Hebeler, and A. Schwenk, *Phys. Rev. D* **86**, 063001 (2012).
- [5] A. Bauswein, T. W. Baumgarte, and H.-T. Janka, *Phys. Rev. Lett.* **111**, 131101 (2013).
- [6] J. Antoniadis, P. C. C. Freire, N. Wex, T. M. Tauris, R. S. Lynch, M. H. van Kerkwijk, M. Kramer, C. Bassa, V. S. Dhillon, T. Driebe, et al., *Science* **340**, 448 (2013).
- [7] H. T. Cromartie et al., *Nat. Astron.* **4**, 72 (2019).
- [8] B. P. Abbott, R. Abbott, T. D. Abbott, F. Acernese, K. Ackley, C. Adams, T. Adams, P. Addesso, R. X. Adhikari, V. B. Adya, et al. (LIGO Scientific Collaboration and Virgo Collaboration), *Phys. Rev. Lett.* **119**, 161101 (2017).
- [9] T. Fischer, N.-U. F. Bastian, M.-R. Wu, P. Baklanov, E. Sorokina, S. Blinnikov, S. Typel, T. Klähn, and D. B. Blaschke, *Nature Astronomy* **2**, 980 (2018).
- [10] A. Bauswein, N.-U. F. Bastian, D. B. Blaschke, K. Chatziioannou, J. A. Clark, T. Fischer, and M. Oertel, *Phys. Rev. Lett.* **122**, 061102 (2019).
- [11] T. Klähn and T. Fischer, *Astrophys. J.* **810**, 134 (2015).
- [12] Y. Nambu and G. Jona-Lasinio, *Phys. Rev.* **122**, 345 (1961).
- [13] S. Klevansky, *Rev. Mod. Phys.* **64**, 649 (1992).
- [14] M. Hempel and J. Schaffner-Bielich, *Nucl. Phys. A* **837**, 210 (2010).
- [15] S. Typel, G. Röpke, T. Klähn, D. Blaschke, and H. H. Wolter, *Phys. Rev. C* **81**, 015803 (2010).
- [16] M. Hempel, T. Fischer, J. Schaffner-Bielich, and M. Liebendörfer, *Astrophys. J.* **748**, 70 (2012).
- [17] T. Klähn, T. Fischer, and M. Hempel, *Astrophys. J.* **836**, 89 (2017).
- [18] S. Banik, M. Hempel, and D. Bandyopadhyay, *Astrophys. J. Supp.* **214**, 22 (2014).
- [19] M. Fortin, M. Oertel, and C. Providência, *Publications of the Astronomical Society of Australia* **35** (2018).
- [20] M. Marques, M. Oertel, M. Hempel, and J. Novak, *Phys. Rev. C* **96**, 045806 (2017).
- [21] S. Typel, *Phys. Rev. C* **71**, 064301 (2005).
- [22] D. Alvarez-Castillo, A. Ayriyan, S. Benic, D. Blaschke, H. Grigorian, and S. Typel, *European Physical Journal A* **52**, 69 (2016).
- [23] A. Akmal, V. R. Pandharipande, and D. G. Ravenhall, *Phys. Rev. C* **58**, 1804 (1998).
- [24] S. Goriely, N. Chamel, and J. M. Pearson, *Phys. Rev. C* **82**, 035804 (2010).
- [25] R. B. Wiringa, V. Fiks, and A. Fabrocini, *Phys. Rev. C* **38**, 1010 (1988).
- [26] J. M. Lattimer and F. Douglas Swesty, *Nuclear Physics A* **535**, 331 (1991).
- [27] G. Shen, C. J. Horowitz, and S. Teige, *Phys. Rev. C* **83**, 035802 (2011).
- [28] G. A. Lalazissis, J. König, and P. Ring, *Phys. Rev. C* **55**, 540 (1997).
- [29] F. Douchin and P. Haensel, *Astron. Astrophys.* **380**, 151 (2001).
- [30] A. W. Steiner, M. Hempel, and T. Fischer, *Astrophys. J.* **774**, 17 (2013).
- [31] Y. Sugahara and H. Toki, *Nuclear Physics A* **579**, 557 (1994).
- [32] H. Toki, D. Hirata, Y. Sugahara, K. Sumiyoshi, and I. Tanihata, *Nuclear Physics A* **588**, 357 (1995).
- [33] J. S. Read, B. D. Lackey, B. J. Owen, and J. L. Friedman, *Phys. Rev. D* **79**, 124032 (2009).
- [34] H. Mütter, M. Prakash, and T. L. Ainsworth, *Physics Letters B* **199**, 469 (1987).
- [35] M. Alford, M. Braby, M. Paris, and S. Reddy, *Astrophys. J.* **629**, 969 (2005).
- [36] B. D. Lackey, M. Nayyar, and B. J. Owen, *Phys. Rev. D* **73**, 024021 (2006).
- [37] M. A. R. Kaltenborn, N.-U. F. Bastian, and D. B. Blaschke, *Phys. Rev. D* **96**, 056024 (2017).
- [38] N.-U. Bastian, D. Blaschke, T. Fischer, and G. Röpke, *Universe* **4**, 67 (2018).
- [39] M. Cierniak, T. Klähn, T. Fischer, and N.-U. Bastian, *Universe* **4**, 30 (2018).
- [40] L. Engvik, E. Osnes, M. Hjorth-Jensen, G. Bao, and E. Ostgaard, *Astrophys. J.* **469**, 794 (1996).
- [41] N. K. Glendenning, *Astrophys. J.* **293**, 470 (1985).
- [42] A. S. Schneider, C. Constantinou, B. Muccioli, and M. Prakash, *Phys. Rev. C* **100**, 025803 (2019).
- [43] P. Danielewicz, R. Lacey, and W. G. Lynch, *Science* **298**, 1592 (2002).
- [44] C. Y. Tsang, M. B. Tsang, P. Danielewicz, W. G. Lynch, and F. J. Fattoyev, *ArXiv e-prints* (2018), 1807.06571.
- [45] J. M. Lattimer and Y. Lim, *Astrophys. J.* **771**, 51 (2013).
- [46] M. Oertel, M. Hempel, T. Klähn, and S. Typel, *Reviews of Modern Physics* **89**, 015007 (2017).
- [47] T. Krüger, I. Tews, K. Hebeler, and A. Schwenk, *Phys. Rev. C* **88**, 025802 (2013).
- [48] Z. Arzoumanian, A. Brazier, S. Burke-Spolaor, S. Chamberlain, S. Chatterjee, B. Christy, J. M. Cordes, N. J. Cornish, F. Crawford, H. Thankful Cromartie, et al., *Astrophys. J. Supp.* **235**, 37 (2018).
- [49] A. Bauswein, O. Just, H.-T. Janka, and N. Stergioulas, *Astrophys. J. Lett.* **850**, L34 (2017).
- [50] S. De, D. Finstad, J. M. Lattimer, D. A. Brown, E. Berger, and C. M. Biwer, *Phys. Rev. Lett.* **121**, 091102 (2018), 1804.08583.
- [51] B. P. Abbott, R. Abbott, T. D. Abbott, F. Acernese, K. Ackley, C. Adams, T. Adams, P. Addesso, R. X. Adhikari, V. B. Adya, et al., *Phys. Rev. Lett.* **121**, 161101 (2018).
- [52] D. S. Balsara, *Journal of Computational Physics* **121**, 357 (1995).
- [53] K. Hotokezaka, K. Kyutoku, H. Okawa, M. Shibata, and K. Kiuchi, *Phys. Rev. D* **83**, 124008 (2011).
- [54] F. Zappa, S. Bernuzzi, D. Radice, A. Perego, and T. Dietrich, *Phys. Rev. Lett.* **120**, 111101 (2018).
- [55] S. Köppel, L. Bovard, and L. Rezzolla, *Astrophys. J. Lett.* **872**, L16 (2019).
- [56] M. Agathos, F. Zappa, S. Bernuzzi, A. Perego, M. Breschi, and D. Radice, *Phys. Rev. D* **101**, 044006 (2020).
- [57] S. Bernuzzi, M. Breschi, B. Daszuta, A. Endrizzi, D. Logoteta, V. Nedora, A. Perego, D. Radice, F. Schianchi, F. Zappa, et al., *Mon. Not. Roy. Astron. Soc.* **497**, 1488 (2020).
- [58] K. Kiuchi, K. Kyutoku, M. Shibata, and K. Taniguchi, *Astrophys. J. Lett.* **876**, L31 (2019).